6th European Conference on Computational Mechanics (ECCM 6)
7th European Conference on Computational Fluid Dynamics (ECFD 7)
1115 June 2018, Glasgow, UK

NUMERICAL SIMULATIONS OF IMMISCIBLE GENERALISED NEWTONIAN FLUIDS

KNUT SVERDRUP[1], NIKOS NIKIFORAKIS[2] AND ANN ALMGREN[3]

[1] Centre for Scientific Computing, University of Cambridge
JJ Thomson Avenue, Cambridge, CB3 0HE, United Kingdom
ksk38@cam.ac.uk

[2] Centre for Scientific Computing, University of Cambridge
JJ Thomson Avenue, Cambridge, CB3 0HE, United Kingdom
nn10005@cam.ac.uk

[3] Center for Computational Sciences and Engineering, Lawrence Berkeley National Laboratory
1 Cyclotron Rd, Berkeley, CA 94720, USA
asalmgren@lbl.gov

Key words: Fluid-Fluid Displacement, Non-Newtonian Yield Stress Fluids, High Performance Computing

Abstract. We present a numerical methodology for three-dimensional large-scale simulations of two-fluid flow for generalised Newtonian fluids exhibiting non-Newtonian behaviour such as a non-zero yield stress and power-law dependency on strain-rate. The incompressible continuity and Cauchy momentum equations, along with appropriate rheological models, are solved using a computational framework initially developed at Lawrence Berkeley National Laboratory. The solver uses second-order Godunov methodology for the advective terms and semi-implicit diffusion in the context of an approximate projection method to evolve the system in time. We have extended the algorithm to enable the simulation of Herschel-Bulkley fluids by means of a mathematical regularisation of the constitutive equation which describes the fluid rheology. Additionally, interfaces between fluids with different properties are treated using a passively advected indicator function. The performance of the software is validated for two-dimensional displacement flow and tested on a three-dimensional viscoplastic dambreak.

1 INTRODUCTION

Fluid dynamics systems involving more than one fluid are countless, and many are so heavily characterised by the interactions that their inclusion in the system description is essential in order to understand it. For this reason, mathematical modeling and numerical simulation of several fluids has been actively researched for the last half century. Noh and Woodward [1] first introduced the advection of a scalar function used to indicate the volume fraction of each fluid in a cell, a method which was named the Volume Of

Fluid (VOF) method by Hirt and Nichols [2] in 1981. Further development of the method by Sussman et al. allowed coupling to level-set methods [3], adaptive mesh hierarchies [4] and three-dimensional flow [5]. Gueyffier et al. added the ability to deal with topology changes through smoothed surface stress methods [6], while Ménard, Tanguy and Berlemont combined VOF with the ghost fluid method for gas interactions [7]. As such, the methodology is mature, versatile and well-documented, and is implemented in major commercial software suites for CFD. However, the application to viscoplastic fluids is limited, and, for the three-dimensional case, does not exist to the best knowledge of the author.

Viscoplastic fluids are non-Newtonian fluids which are characterised by a minimum induced stress necessary for flow to occur. For this reason they are also commonly referred to as yield-stress fluids. When the imposed stress does not exceed the threshold value, the material is modelled as a rigid solid. In regions where the yield stress is exceeded, however, the material flows with a finite viscosity. The ability of the material to support a stress under certain circumstances gives rise to phenomena such as non-flat surfaces at rest under gravity and the coexistence of yielded (flowing) and unyielded (rigid) regions within the fluid. The former can be demonstrated by distorting the surface of mayonnaise in a jar: gravity alone is not strong enough to surpass the yield stress, and the surface remains in its distorted state. In addition to being fundamentally interesting from the perspectives of rheology, fluid mechanics and mathematical modelling, yield stress fluids occur naturally and are paramount to the success of animals such as mudskippers [8] and snails [9]. Their importance in industries ranging from medicine [10, 11, 12, 13] to oil and gas exploration [14, 15, 16] has led to extensive research contributions in the field. For further reading on developments in viscoplastic fluids, we refer the reader to the review papers by Barnes [17] and Balmforth et al. [18].

Just as for Newtonian fluids, the pursuit of knowledge about viscoplastic fluids has relied heavily on computational methods in the last fifty years. Compared to the Newtonian case, however, the numerical simulations are much more computationally intensive. In order to remedy this, we recently extended the state-of-the-art open-source code IAMR to allow simulation of Herschel-Bulkley fluids evolving in time and three spatial dimensions [19]. IAMR uses a second-order accurate, approximate projection method to solve the incompressible Navier-Stokes equations [20]. The code is built on the AMReX (`https://amrex-codes.github.io`) software framework for developing massively parallel block-structured AMR applications. By using this as our software framework, we are able to take full advantage of modern supercomputer architectures in our simulations.

Presently, we further extend the capabilities of the IAMR code, to systems containing multiple generalised Newtonian fluids. This necessitates the use of a passively advected scalar to indicate the locations of each fluid as the system evolves in time. To ensure that the two-fluid extension works as expected, we validate our code against the two-dimensional displacement flow of a Bingham fluid by a Newtonian fluid along a plane channel. When the yield stress of the Bingham fluid is high enough, this generates static wall layers, as illustrated by Wielage-Burchard and Frigaard [21]. Moreover, we illustrate the capabilities of our code by simulating the collapse of a three-dimensional cube of

high-density Herschel-Bulkley fluid surrounded by a lower-density Newtonian.

A brief outline of the remainder of the paper is as follows. In section 2, we introduce the governing equations and rheological model employed to describe our system, and the methodology for modeling the immiscible flow of two fluids. Section 3 contains an explanation of the numerical algorithm which we utilise. Our simulations are validated through comparisons with reference displacement flows in a plane channel in section 4, in addition to being further evaluated by computing a fully three-dimensional viscoplastic dam-break. Section 5 concludes the paper.

2 MATHEMATICAL FORMULATION

We denote by $\rho(\boldsymbol{x}, t)$ the material density. The velocity field is introduced as $\boldsymbol{u}(\boldsymbol{x}, t)$, with components u, v and w. The Cauchy stress tensor $\boldsymbol{\sigma}$ is defined as a sum of isotropic and deviatoric parts, $\boldsymbol{\sigma} = -p\mathbf{I} + \boldsymbol{\tau}$. Here, the pressure $p(\boldsymbol{x}, t)$ is multiplied by the identity tensor, while the deviatoric part of the stress tensor is denoted $\boldsymbol{\tau}(\boldsymbol{x}, t)$. In order to describe immiscible two-fluid flow, we introduce a passive scalar $\lambda(\boldsymbol{x}, t) \in [0, 1]$ which plays the role of an indicator, and let the simulated fluid properties be a function of this indicator. The fluid motion is then governed by

$$\frac{\partial \rho}{\partial t} + \boldsymbol{u} \cdot \nabla \rho = 0, \tag{1}$$

$$\frac{\partial \boldsymbol{u}}{\partial t} + \boldsymbol{u} \cdot \nabla \boldsymbol{u} = \frac{1}{\rho} \left(-\nabla p + \nabla \cdot \boldsymbol{\tau} \left(|\dot{\boldsymbol{\gamma}}|, \lambda \right) + \boldsymbol{f} \right), \tag{2}$$

$$\frac{\partial \lambda}{\partial t} + \boldsymbol{u} \cdot \nabla \lambda = 0, \tag{3}$$

$$\nabla \cdot \boldsymbol{u} = 0, \tag{4}$$

completed by a suitable constitutive equation $\boldsymbol{\tau}\left(|\dot{\boldsymbol{\gamma}}|, \lambda\right)$. Here, we have introduced $\boldsymbol{f}$ to describe external body forces such as gravity acting on the fluid, in addition to the rate-of-strain tensor $\dot{\boldsymbol{\gamma}} = \frac{1}{2}\left(\nabla \boldsymbol{u} + \nabla \boldsymbol{u}^{\top}\right)$. Note that we take the tensor norm induced by the Frobenius inner product, $|\dot{\boldsymbol{\gamma}}| = \sqrt{\mathrm{tr}(\dot{\boldsymbol{\gamma}}\dot{\boldsymbol{\gamma}}^{\top})}$ (and similar for $|\boldsymbol{\tau}|$). Equations (1)-(4) constitute variable density conservation of mass, Cauchy momentum balance, passive advection of a fluid indicator and the incompressibility constraint. In general, (3) includes a diffusive term proportional to $\nabla^2 \lambda$ on the right hand side, but for the case of immiscible flow which we are studying the coefficient of proportionality is zero. Rheological behaviour is captured by non-Newtonian equations of state where the stress response is dependent on the rate-of-strain tensor $\dot{\boldsymbol{\gamma}}$ and the indicator λ.

Many fluids are accurately modelled by a non-Newtonian behaviour that captures shear-dependency through a smooth increase or decrease in apparent viscosity. Such fluids include pseudoplastics (shear-thinning) and dilatants (shear-thickening). A model which captures this behaviour is the power-law fluid, characterised by its (dimensionless) flow behaviour index n and consistency μ, which has units $\mathrm{Pa\,s}^n$). The Newtonian case with $n = 1$ separates pseudoplastics ($n < 1$) from dilatants ($n > 1$).

Viscoplastic fluids have a stress threshold $\tau_0 > 0$ (the yield stress), below which they do

not flow. The simplest type of viscoplastic fluid is the Bingham fluid [22], characterised by zero strain rate below the yield stress. In the yielded region, however, the stress depends linearly on the rate-of-strain magnitude, just like a Newtonian fluid. For Bingham plastics, we note that the apparent viscosity has a singularity for $\dot{\boldsymbol{\gamma}} = 0$.

In many applications, it is desirable to capture both the yield stress of viscoplastic fluids and the power-law dependency occurring once the fluid starts flowing. A widely used rheological model for such fluids is due to Herschel and Bulkley [23]. The Herschel-Bulkley fluid facilitates a very general description of non-Newtonian fluids, as it is a yield stress fluid with a nonlinear stress-strain dependency in the yielded region. As such, it can be thought of as a hybrid between Bingham plastics and power law fluids. The constitutive equation is

$$\begin{cases} \dot{\boldsymbol{\gamma}} = 0 & \text{if} \quad |\boldsymbol{\tau}| \leq \tau_0 \\ \boldsymbol{\tau} = 2^{\frac{n+1}{2}} \mu |\dot{\boldsymbol{\gamma}}|^{n-1} \dot{\boldsymbol{\gamma}} + \frac{\tau_0}{|\dot{\boldsymbol{\gamma}}|} \dot{\boldsymbol{\gamma}} & \text{if} \quad |\boldsymbol{\tau}| > \tau_0 \end{cases}, \tag{5}$$

where the singularity for zero strain-rate is apparent. Computational schemes such as that in IAMR cannot be used in the presence of such singularities. Regularisation deals with the problem by replacing the ill-behaved apparent viscosity with a function that approximates the rheological behaviour, but which stays bounded for arbitrarily small $\dot{\boldsymbol{\gamma}}$. This is done by introducing an additional parameter ε to the apparent viscosity, which describes how big the effect of the regularisation is. A large value of ε allows for inexpensive computations even near unyielded flow, while the limit $\varepsilon \to 0$ recovers the unregularised description. We employ the popular Papanastasiou regularisation [24], which utilises an exponential relaxation. Introducing the apparent viscosity $\eta(|\dot{\boldsymbol{\gamma}}|)$ through the relation $\boldsymbol{\tau} = 2\eta\dot{\boldsymbol{\gamma}}$, the regularised Herschel-Bulkley model satisfies

$$\eta(|\dot{\boldsymbol{\gamma}}|) = \left(2^{\frac{n-1}{2}} \mu |\dot{\boldsymbol{\gamma}}|^n + \frac{\tau_0}{2}\right) \frac{1 - e^{-|\dot{\boldsymbol{\gamma}}|/\varepsilon}}{|\dot{\boldsymbol{\gamma}}|}. \tag{6}$$

Finally, we need to ensure that the model encapsulates the dependency of the apparent viscosity on which fluid is present at a given point. The extension of viscoplastic flow in the IAMR framework to incorporate several fluids is the main motivation for the present work. For Newtonian fluids, whose viscosity is given by a constant dynamic coefficient μ_i in the fluid i, this is done by linear interpolation based on λ. For a system of two fluids, $i \in \{1, 2\}$, we therefore take

$$\mu(\lambda) = \lambda\mu_1 + (1 - \lambda)\mu_2, \tag{7}$$

so that $\mu = \mu_1$ when $\lambda = 1$ and $\mu = \mu_2$ when $\lambda = 0$. For Herschel-Bulkley fluids, which use two additional parameters to describe the apparent viscosoity, we simply take similar averages to obtain the apparent flow index and yield stress:

$$n(\lambda) = \lambda n_1 + (1 - \lambda)n_2, \tag{8}$$

$$\tau_0(\lambda) = \lambda\tau_{0,1} + (1 - \lambda)\tau_{0,2}. \tag{9}$$

3 NUMERICAL ALGORITHM

An approximate projection method for solving the variable-density incompressible Navier-Stokes equations on an adaptive mesh hierarchy has been implemented in the IAMR code. The algorithm was described for the constant viscosity case by Almgren et al. [20], and the extension to generalised Newtonian viscoplastics is described in Sverdrup et al. [19]. In addition to solving the mass and momentum equations for velocity and pressure, the IAMR code allows for the (conservative or passive) advection of any number of scalar quantities. The implementation is such that the code can be run on architectures from single-core laptops through to massively parallel supercomputers.

In the approximate projection method as implemented in IAMR, an advection-diffusion step is used to advance the velocity in time; the solution is then (approximately) projected onto the space of divergence-free fields. In the advection-diffusion step, (2), is discretized in time to construct a new-time provisional velocity field, $\boldsymbol{u}^*$, without enforcing (4). i.e. we define $\boldsymbol{u}^*$ using

$$\frac{\boldsymbol{u}^* - \boldsymbol{u}^k}{\Delta t} = -[\boldsymbol{u}^{\mathrm{MAC}} \cdot \nabla \tilde{\boldsymbol{u}}]^{k+\frac{1}{2}} + \frac{1}{\rho^{k+\frac{1}{2}}} \left(-\boldsymbol{G}p^{k-\frac{1}{2}} + \frac{1}{2} \left(\nabla \cdot \boldsymbol{\tau}(\boldsymbol{u}^k) + \nabla \cdot \boldsymbol{\tau}(\boldsymbol{u}^*) \right) + \boldsymbol{f}^k \right), \tag{10}$$

where $\boldsymbol{G}p^{k-\frac{1}{2}}$ is a lagged approximation to the pressure gradient ∇p and the density $\rho^{k+\frac{1}{2}}$ is the average of times t^k and t^{k+1}.

The time-centered advective update term, $[\boldsymbol{u}^{\mathrm{MAC}} \cdot \nabla \tilde{\boldsymbol{u}}]^{k+\frac{1}{2}}$ is constructed using an unsplit second-order accurate upwind scheme. All velocity components are predicted from cell centers at time t^k to faces at time $t^{k+\frac{1}{2}}$ using Taylor series approximations to define $\tilde{\boldsymbol{u}}$. The face-centered normal velocities are then projected to be divergence-free to define $\boldsymbol{u}^{\mathrm{MAC}}$. These velocities are also employed to advect the scalars, for which separate Taylor approximations are computed. Equations (1) and (3) are therefore advanced through solving

$$\frac{\rho^{k+1} - \rho^k}{\Delta t} = -[\boldsymbol{u}^{\mathrm{MAC}} \cdot \nabla \tilde{\rho}]^{k+\frac{1}{2}}, \tag{11}$$

$$\frac{\lambda^{k+1} - \lambda^k}{\Delta t} = -[\boldsymbol{u}^{\mathrm{MAC}} \cdot \nabla \tilde{\lambda}]^{k+\frac{1}{2}}. \tag{12}$$

In order to compute the explicit viscous term, $\boldsymbol{\tau}(\boldsymbol{u}^k)$, we must first evaluate the viscosity parameters according to (7)-(9), taking λ^k as input. Subsequently, we evaluate the stress using velocity components at time t^k, i.e. we define $\dot{\boldsymbol{\gamma}}^k = \dot{\boldsymbol{\gamma}}(\boldsymbol{u}^k)$, $\eta^k = \eta(|\dot{\boldsymbol{\gamma}}^k|)$ and write $\boldsymbol{\tau}(\boldsymbol{u}^k) = 2\eta^k \, \dot{\boldsymbol{\gamma}}^k$.

We solve for $\boldsymbol{u}^*$ with the same η^k, i.e.

$$\left(\boldsymbol{u}^* - \frac{\Delta t}{\rho} \nabla \cdot (\eta^k \, \dot{\boldsymbol{\gamma}}^*) \right) = \boldsymbol{u}^k - \Delta t [\boldsymbol{u}^{\mathrm{MAC}} \cdot \nabla \tilde{\boldsymbol{u}}]^{k+\frac{1}{2}} + \frac{\Delta t}{\rho^{k+\frac{1}{2}}} \left(-\boldsymbol{G}p^{k-\frac{1}{2}} + \nabla \cdot (\eta^k \dot{\boldsymbol{\gamma}}^k) + \boldsymbol{f}^k \right). \tag{13}$$

Note that all velocity components are solved for simultaneously.

The final part of the algorithm is the projection step and subsequent pressure update. The velocity field $\boldsymbol{u}^*$ does not in general satisfy the divergence constraint as given by (4). We solve

$$L_\rho \phi = D\left(\frac{1}{\Delta t}\,\boldsymbol{u}^* + \frac{1}{\rho}\,\boldsymbol{G}p^{k-\frac{1}{2}}\right) \tag{14}$$

where D is a discrete divergence and $\boldsymbol{G}$ a discrete gradient. L_ρ is a second-order accurate approximation to $\nabla \cdot \frac{1}{\rho^{k+1/2}}\nabla$. The new-time velocity is then defined by

$$\boldsymbol{u}^{k+1} = \boldsymbol{u}^* - \Delta t \frac{1}{\rho^{k+\frac{1}{2}}}\boldsymbol{G}\phi \tag{15}$$

and the updated pressure by

$$p^{k+\frac{1}{2}} = \phi \ . \tag{16}$$

4 SIMULATION RESULTS

4.1 Validation: plane channel displacement

As a validation problem, we consider the displacement of a Bingham fluid by a Newtonian in a plane channel, as described by Wielage-Burchard and Frigaard [21]. Our domain is a two-dimensional duct of width $2\mathcal{W}$ and length $\mathcal{L}$. Through the duct, there is a flow with mean x-velocity $\mathcal{U}$ across its width. In the absence of external forces, this corresponds to a plane Poiseuille flow, for which analytical solutions exist both for Newtonian and Bingham fluids. Initially, the domain is filled with a Bingham fluid, indicated by $\lambda = 1$. The properties of this fluid are $\mu_1 = 1\,\mathrm{Pa\,s}$ and $\tau_{0,1} = 100\sqrt{2}\,\mathrm{Pa}$. We initialise the velocity profile as the steady-state analytical solution for Bingham fluids, given by

$$u(y) = u_{\max,1} \cdot \begin{cases} 1, & |y| \le y_0, \\ 1 - \left(\frac{|y|-y_0}{\mathcal{W}-y_0}\right)^2, & y_0 < |y| \le \mathcal{W}, \end{cases} \tag{17}$$

where

$$u_{\max,1} = \frac{(\mathcal{W}-y_0)^2}{2y_0} \cdot \frac{\tau_{0,1}}{\sqrt{2}\mu_1} \tag{18}$$

is the maximum velocity of the fluid, occurring in the plug region $|y| < y_0$. The characteristic distance y_0 is found by demanding $\frac{1}{\mathcal{W}}\int_0^{\mathcal{W}} u(y)\mathrm{d}y = \mathcal{U}$, resulting in the cubic equation

$$\left(\frac{y_0}{\mathcal{W}}\right)^3 - 3\left(1 + \frac{2\sqrt{2}\mu_1\mathcal{U}}{3\tau_{0,1}\mathcal{W}}\right)\frac{y_0}{\mathcal{W}} + 2 = 0. \tag{19}$$

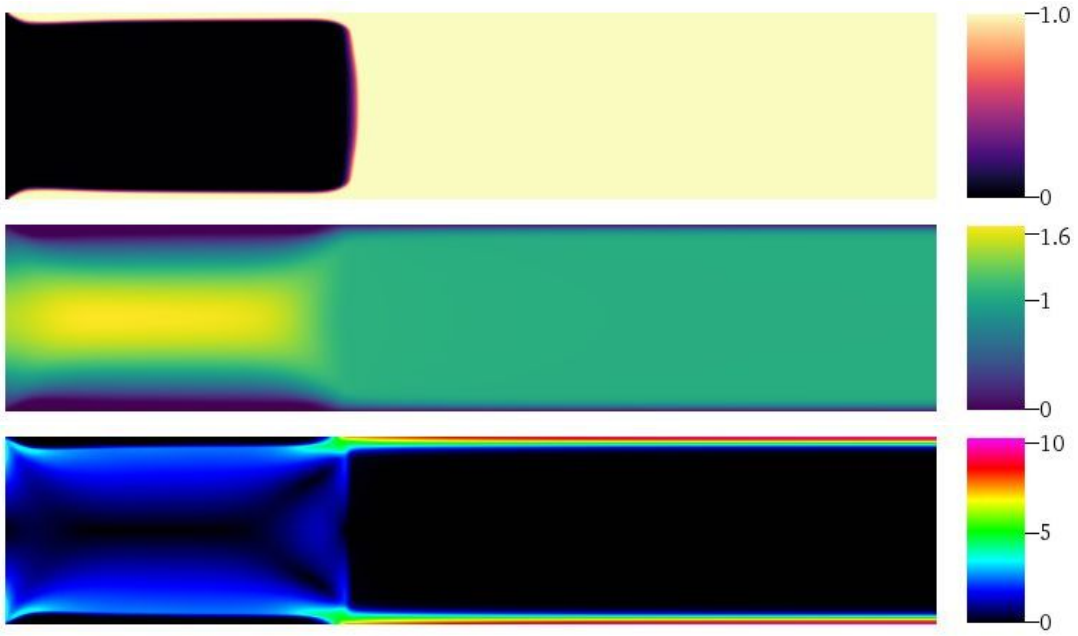

Figure 1: Snapshots of the plane channel displacement flow at $t = 3.4\,\mathrm{s}$, depicting the indicator (top, dimensionless), x-velocity (middle, m/s) and strain-rate magnitude (bottom, s^{-1}). In each case, the distribution in the full duct $[0, \mathcal{L}] \times [-\mathcal{W}, \mathcal{W}]$ is shown.

At time $t = 0$, we inject a Newtonian fluid with dynamic viscosity $\mu_2 = 10\,\mathrm{Pa\,s}$ at the left-hand side of the duct. This is achieved through an inflow boundary condition where $\lambda = 2$ and the velocity profile is

$$u(y) = u_{\max,2}\left(1 - \left(\frac{y}{\mathcal{W}}\right)^2\right) \tag{20}$$

with $u_{\max,2} = \frac{3}{2}\mathcal{U}$.

We set $\mathcal{W} = 1\,\mathrm{m}$, $\mathcal{L} = 10\,\mathrm{m}$, $\mathcal{U} = 1\,\mathrm{m/s}$, $\varepsilon = 1/200$ and use 128 cells across the channel width to obtain high-resolution heatmaps. Figure 1 shows the resulting distributions of the indicator λ, velocity u and strain-rate magnitude $|\dot{\boldsymbol{\gamma}}|$ after 3.4 s. Note that due to the high Bingham number, residual wall layers of fluid 2 remain along the top and bottom walls. The velocity profile follows the Bingham profile downstream of the displacement front (for this case, we have $y_0 \approx 0.86\mathcal{W}$), while a quadratic profile develops between the stationary residual wall layers upstream of the front.

In order to obtain a quantitative comparison with the results of Wielage-Burchard and Frigaard [21], we run the simulation until steady-state with 32 cells across the channel width. Slices through the centre of the domain are shown in figure 2, with their results superimposed. As is evident, there is excellent agreement between our model and the reference.

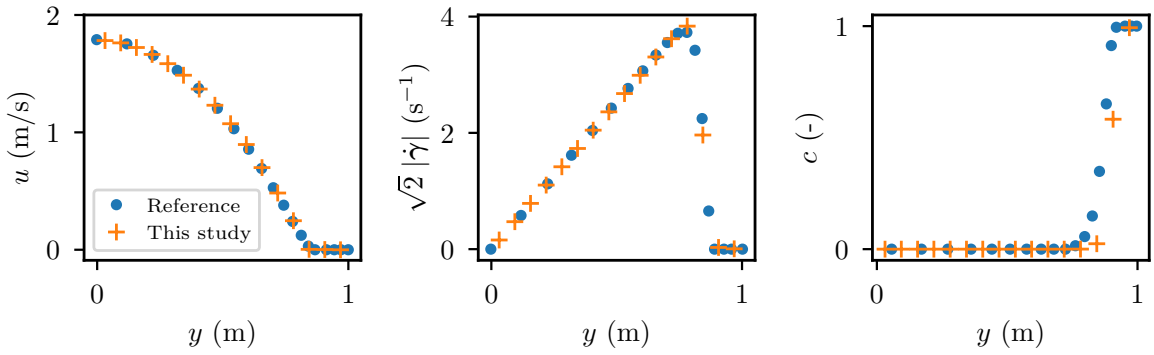

Figure 2: Comparisons of plane channel displacement results with Wielage-Burchard and Frigaard [21] for validation of our code. We look at the variation at $x = 5$. Our indicator function is sharper than the reference, but we obtain the same static layer width, as is evident from the profiles of x-velocity and strain-rate magnitude.

4.2 Evaluation: three-dimensional viscoplastic dam-break

As a more severe test case of our software's capabilities, we consider the collapse of a square prism of heavy, viscous fluid under a downward-acting vertical force, inspired by the two-dimensional system studied by Liu et al. [25]. The square prism is initialised with side lengths $\mathcal{S} = 1\,\mathrm{m}$ and height $\mathcal{H} = 1\,\mathrm{m}$ in the centre of our domain, within which the fluid properties are $\rho_1 = 1000\,\mathrm{kg/m^3}$ and $\mu_1 = 10^{-2}\,\mathrm{Pa\,s}$. Surrounding the heavy mass is a lighter fluid with $\rho_2 = 1\,\mathrm{kg/m^3}$ and $\mu_2 = 10^{-3}\,\mathrm{Pa\,s}$. We introduce a forcing term $\boldsymbol{f} = \rho f \hat{\boldsymbol{z}}$ and let $f = 0.004\,\mathrm{m/s}$. Results for the Newtonian case are shown in figure 3. A second simulation is performed where the collapsing prism is a Herschel-Bulkley fluid with $n_1 = 0.5$ and $\tau_{0,1} = 5 \cdot 10^{-3}\,\mathrm{Pa}$. The corresponding results are shown in 4. Note how much slower the flow is, and how the mass retains its shape to a much greater degree. Due to the yield stress, the heavier will eventually cease to flow, without obtaining a flat surface. This initial dambreak test shows expected behaviour qualitatively, but the system certainly warrants further investigation.

5 CONCLUSIONS

We have successfully implemented a numerical model for two-fluid flows for generalised Newtonians within the highly parallelisable software framework IAMR, and validated our results against a benchmark test of two-dimensional displacement flow in a plane channel. The non-Newtonian rheology, which is described using the Herschel-Bulkley model, is handled using mathematical regularisation, while the fluid-fluid interfaces are tracked using a passively advected indicator function. Further to the brief validation study, we have started initial experiments with the more demanding test case of viscoplastic dambreaks in three dimensions. Future work will focus on thorough verification of the code, and utilisation of adaptive mesh refinement (readily available in IAMR) to enhance simulation accuracy and efficiency.

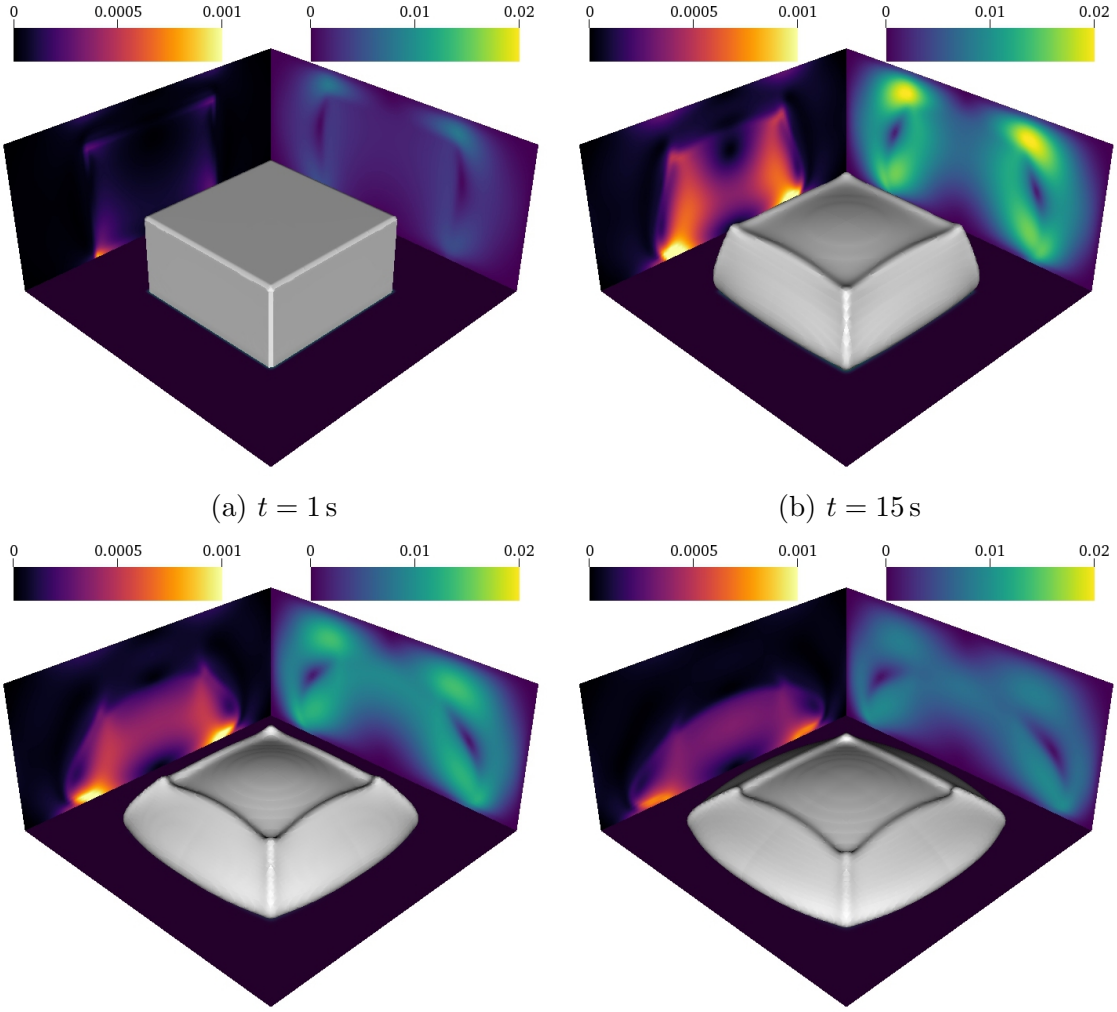

(a) $t = 1\,\mathrm{s}$ (b) $t = 15\,\mathrm{s}$

(c) $t = 30\,\mathrm{s}$ (d) $t = 46\,\mathrm{s}$

Figure 3: Three-dimensional Newtonian dambreak. The contour surface $\lambda = 0.5$ shows the interface between the heavier, more viscous fluid and the surrounding lighter one. On the back left wall, a slice through $x = 0$ is depicted of the stress, while the back right wall shows the velocity magnitude in the slice $y = 0$.

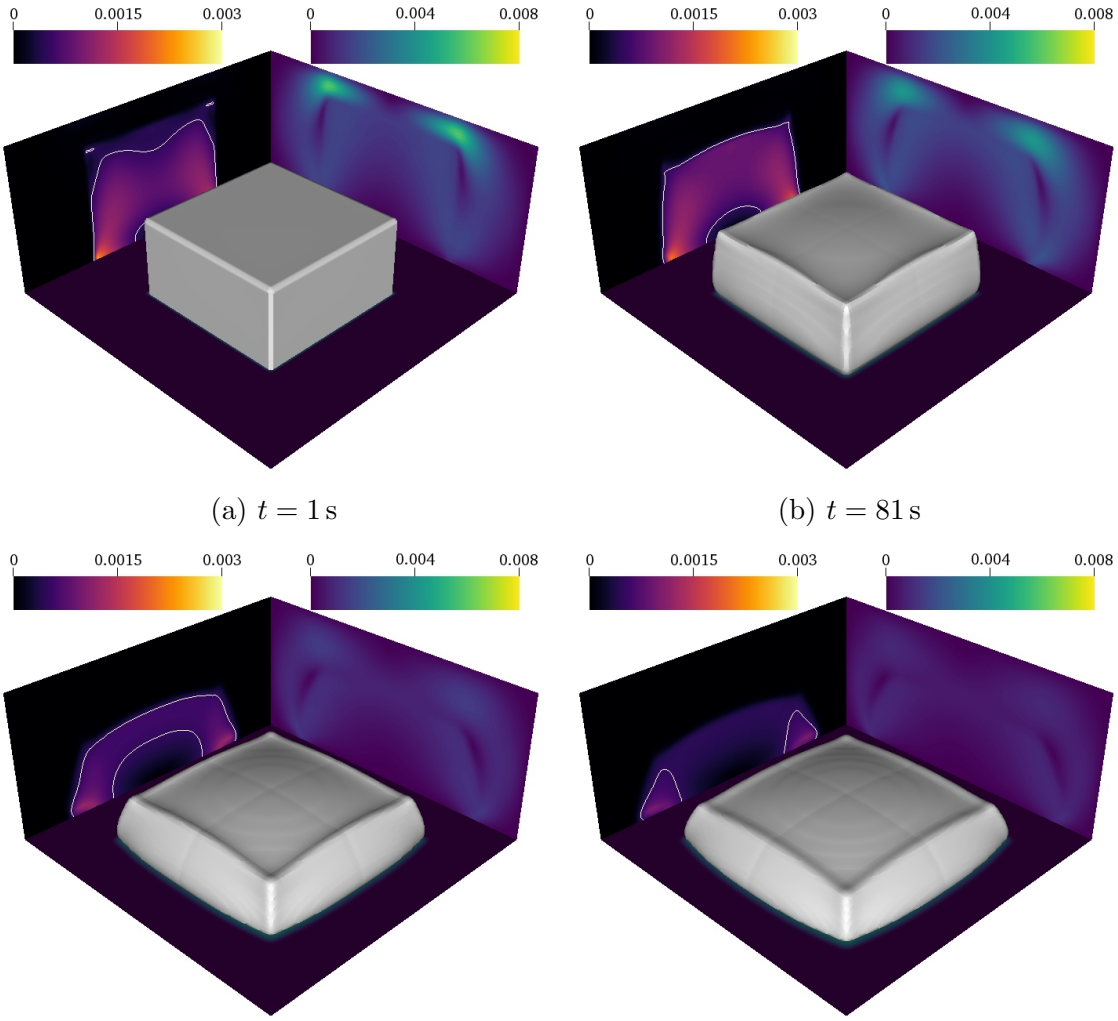

(a) $t = 1\,\mathrm{s}$ (b) $t = 81\,\mathrm{s}$

(c) $t = 269\,\mathrm{s}$ (d) $t = 386\,\mathrm{s}$

Figure 4: Three-dimensional viscoplastic dambreak. The contour surface $\lambda = 0.5$ shows the interface between the heavier Herschel-Bulkleyand the surrounding Newtonian. On the back left wall, a slice through $x = 0$ is depicted of the stress, with the yield surface $|\boldsymbol{\tau}| = \tau_0$ shown as a single white line. The back right wall shows the velocity magnitude in the slice $y = 0$.

Knut Sverdrup would like to acknowledge the EPSRC Centre for Doctoral Training in Computational Methods for Materials Science for funding under grant number EP/L015552/1. Additionally, he acknowledges the funding and technical support from BP through the BP International Centre for Advanced Materials (BP-ICAM) which made this research possible.

REFERENCES

[1] Noh, W. F. & Woodward, P. SLIC (simple line interface calculation). In *Proceedings of the fifth international conference on numerical methods in fluid dynamics June 28–July 2, 1976 Twente University, Enschede, Netherlands*, 330–340 (Springer, 1976).

[2] Hirt, C. W. & Nichols, B. D. Volume of fluid (VOF) method for the dynamics of free boundaries. *Journal of Computational Physics* **39**, 201–225 (1981).

[3] Sussman, M., Smereka, P. & Osher, S. A level set approach for computing solutions to incompressible two-phase flow. *Journal of Computational Physics* **114**, 146–159 (1994).

[4] Sussman, M. *et al.* An adaptive level set approach for incompressible two-phase flows. *Journal of Computational Physics* **148**, 81–124 (1999).

[5] Sussman, M. & Puckett, E. G. A coupled level set and volume-of-fluid method for computing 3D and axisymmetric incompressible two-phase flows. *Journal of Computational Physics* **162**, 301–337 (2000).

[6] Gueyffier, D., Li, J., Nadim, A., Scardovelli, R. & Zaleski, S. Volume-of-fluid interface tracking with smoothed surface stress methods for three-dimensional flows. *Journal of Computational Physics* **152**, 423–456 (1999).

[7] Ménard, T., Tanguy, S. & Berlemont, A. Coupling level set/VOF/ghost fluid methods: Validation and application to 3D simulation of the primary break-up of a liquid jet. *International Journal of Multiphase Flow* **33**, 510–524 (2007).

[8] Pegler, S. S. & Balmforth, N. J. Locomotion over a viscoplastic film. *Journal of Fluid Mechanics* **727**, 1–29 (2013).

[9] Denny, M. W. A quantitative model for the adhesive locomotion of the terrestrial slug, ariolimax columbianus. *Journal of experimental Biology* **91**, 195–217 (1981).

[10] Apostolidis, A. J. & Beris, A. N. Modeling of the blood rheology in steady-state shear flows. *Journal of Rheology* **58**, 607–633 (2014).

[11] Apostolidis, A. J., Armstrong, M. J. & Beris, A. N. Modeling of human blood rheology in transient shear flows. *Journal of Rheology* **59**, 275–298 (2015).

[12] Apostolidis, A. J. & Beris, A. N. The effect of cholesterol and triglycerides on the steady state shear rheology of blood. *Rheologica Acta* **55**, 497–509 (2016).

[13] Apostolidis, A. J., Moyer, A. P. & Beris, A. N. Non-newtonian effects in simulations of coronary arterial blood flow. *Journal of Non-Newtonian Fluid Mechanics* **233**, 155–165 (2016).

[14] Bittleston, S. & Guillot, D. Mud removal: research improves traditional cementing guidelines. *Oilfield Review* **3**, 44–54 (1991).

[15] Taghavi, S., Alba, K., Moyers-Gonzalez, M. & Frigaard, I. Incomplete fluid–fluid displacement of yield stress fluids in near-horizontal pipes: experiments and theory. *Journal of Non-Newtonian Fluid Mechanics* **167**, 59–74 (2012).

[16] Frigaard, I. A., Paso, K. G. & de Souza Mendes, P. R. Bingham's model in the oil and gas industry. *Rheologica Acta* **56**, 259–282 (2017).

[17] Barnes, H. A. The yield stress – a review or $\pi\alpha\nu\tau\alpha$ $\rho\varepsilon\iota$ – everything flows? *Journal of Non-Newtonian Fluid Mechanics* **81**, 133–178 (1999).

[18] Balmforth, N. J., Frigaard, I. A. & Ovarlez, G. Yielding to stress: recent developments in viscoplastic fluid mechanics. *Annual Review of Fluid Mechanics* **46**, 121–146 (2014).

[19] Sverdrup, K., Nikiforakis, N. & Almgren, A. Time-dependent viscoplastic fluid flow simulations in two and three dimensions. *arXiv preprint arXiv:1803.00417* (2018).

[20] Almgren, A., Bell, J., Colella, P., Howell, L. & Welcome, M. A conservative adaptive projection method for the variable density incompressible Navier–Stokes equations. *Journal of Computational Physics* **142**, 1–46 (1998).

[21] Wielage-Burchard, K. & Frigaard, I. Static wall layers in plane channel displacement flows. *Journal of Non-Newtonian Fluid Mechanics* **166**, 245–261 (2011).

[22] Bingham, E. C. An investigation of the laws of plastic flow. *Bulletin of the Bureau of Standards* **13**, 309–353 (1916).

[23] Herschel, W. H. & Bulkley, R. Konsistenzmessungen von gummi-benzollösungen. *Colloid & Polymer Science* **39**, 291–300 (1926).

[24] Papanastasiou, T. C. Flows of materials with yield. *Journal of Rheology* **31**, 385–404 (1987).

[25] Liu, Y., Balmforth, N., Hormozi, S. & Hewitt, D. Two–dimensional viscoplastic dambreaks. *Journal of Non-Newtonian Fluid Mechanics* **238**, 65–79 (2016).